Journal of Materials Chemistry A

Accepted Manuscript

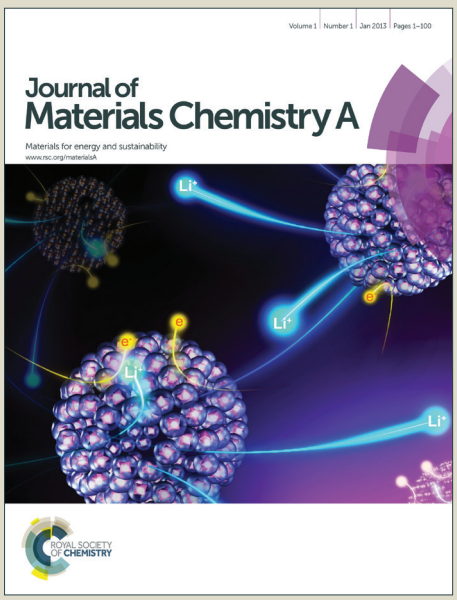

ROYAL SOCIETY OF CHEMISTRY

www.rsc.org/materialsA

Graphical Table of Contents

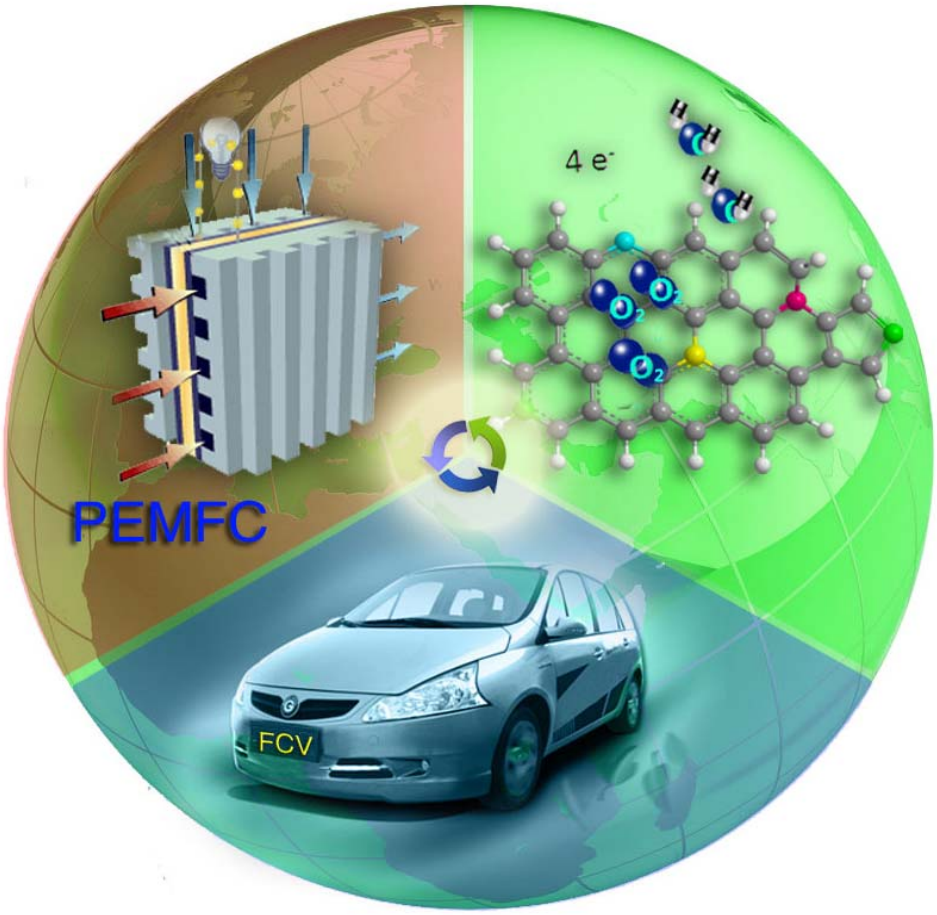

Nitrogen-doped porous carbon electrocatalysts (PNCEs) with hierarchically porous structure have been synthesized from polyaniline (PANI)-polyvinylpyrrolidone (PVP) composite by the chemical polymerization combining the high temperature pyrolysis in presence of ammonium. The PNCEs displays the best performance achieving a maximum power density of 456 mW cm^{-2} and ORR onset potential of 0.90 V. More prominently, the catalyst presents superior stability as well as tolerance of methanol and SO_2 to the commercial JM-Pt/C catalyst in 0.5 M H_2SO_4.

Cite this: DOI: 10.1039/c0xx00000x

www.rsc.org/xxxxxx

ARTICLE TYPE

Nitrogen-doped Hierarchically Porous Carbon as Efficient Oxygen Reduction Electrocatalysts in Acid Electrolyte

Hexiang Zhong,*[a] Chengwei Deng[a,b], Yanling Qiu[a] , Lan Yao[a,b] and Huamin Zhang*[a]

Received (in XXX, XXX) Xth XXXXXXXXX 20XX, Accepted Xth XXXXXXXXX 20XX

DOI: 10.1039/b000000x

Nitrogen-doped carbon was found exhibiting excellent activity as electrocatalyst in renewable energy devices. A controllable method to synthesize N-doped hierarchically porous carbons (PNCEs) partly with graphene-like structure by using polyaniline (PANI)-polyvinylpyrrolidone (PVP) composite as a carbon source via a soft-template process is reported. The catalytic mechanism is thoroughly studied to better understand the relationship between the structure, Fe species and catalytic activity. The PNCEs prepared at 1000 ^{o}C displays the best performance achieving a maximum power density of 456 mW cm^{-2} and oxygen reduction reaction (ORR) onset potential of 0.90 V. More prominently, the catalyst presents superior stability as well as poison tolerance including methanol and SO_2 to the commercial JM-Pt/C catalyst in 0.5 M H_2SO_4. The PVP is proved to tailor the structure, improve the surface area, and alter the transition metal species. The PNCEs synthesized under NH_3 exhibit much better catalytic activity toward ORR compared to the undoped carbon and PNCEs synthesized under N_2 atmosphere. Furthermore, it is found the nitrogen bonding configurations, textural structure, Fe species and surface areas of PNCEs play key roles in the electrocatalytic activity towards the ORR. The forming FeN_4 species hosted in the micropores acts as the active component for ORR activity on PNCEs although it is not the only contributors of the high performance of PNCEs. The catalyst is expected to be a promising non-noble electrocatalyst for polymer electrolyte membrane fuel cells.

Introduction

Among various alternative energy sources, polymer electrolyte membrane fuel cells (PEFCs) have attracted considerable attention because of their high power density, high efficiency, and environmental friendliness.[1] They have been successfully demonstrated in many fields, but the issues such as cost, stability and reliability still hamper their final commercialization.[2] Platinum-based catalyst has been regarded as the most widely-used electrocatalyst in PEFCs due to its high catalytic activity and excellent stability in acid environments. [3,4] However, platinum as a precious noble metal is expensive and resource-limited, which contributes to the high cost of PEFCs vehicles. Thus, the development of low-cost oxygen reduction reaction (ORR) eletrocatalysts with high catalytic activity and stability is crucial to overcome the drawbacks of the present Pt/C electrocatalysts. In addition, because ambient air is compressed directly into the cathode as the oxidant in the fuel cell vehicles, the performance and durability of the PEFCs depend significantly on the quality of the ambient air. With the deterioration in environmental pollution, the poison of the Pt/C electrocatalysts caused by the impurities in the air including the SO_2, NO_x also results in the catalyst poison and significant deterioration of the PEFCs performance.[5] Moreover, in the PEFCs with methanol as fuel, the Pt/C catalysts are easily poisoned by the methanol. Therefore, the exploration of the cheap, abundant non-noble catalysts with high activity and stability as well as high poison-tolerance is significantly required.

Porous carbon materials have many specific features such as high surface area, thermal and chemical stability, and good electrical conductivities etc. The incorporation of heteroatom such as nitrogen, boron, sulphur and so on into the carbon framework can significantly alter their conducting, catalytic, band storage properties.[4a, 6] These materials exhibit high thermal and mechanical stability as well as prominent catalytic properties, which make them attractive choices in many potential applications, primarily in the field of renewable energy.[7,8] Since Gong et al.[9] reported the high ORR activity of nitrogen-doped carbon nanotubes in 2009, the nitrogen-doped carbon catalysts have been widely investigated as ORR catalysts in PEFCs. Many of the carbon based catalysts such as nitrogen-doped graphite, CNT, graphene and so on, present superior or comparable activity and stability to Pt/C catalysts in the alkaline electrolyte fuel cells. [10] However, most of these materials present high overpotential and comparatively lower activity to Pt/C catalysts in acid electrolyte fuel cells. Thus, the development of nitrogen-doped carbon materials functioning in acidic solutions is urgently needed for the development of practical applications.

The polymers such as polypyrrole, poly (p-phenylene), polypyrrolidone, polyacrylonitrile and polyaniline have been widely used for the preparation of carbon materials.[11] Among them, polyaniline (PANI) has been regarded as an attractive precursor for synthesis of activated carbon catalysts due to its high conductivity, unique redox tunability, high stability, high surface area and network structure.[12] Kim et al.[13] has synthesized the polyaniline-based mesoporous carbons with the SiO_2 as template. The resultant carbon presented high electrochemical performance in capacitor. Silva et al.[14] reported the ORR activity of metal-containing O-doped carbon or N-doped carbon, which was synthesized by pyrolysis of PANI/SBA-15 composite material under nitrogen atmosphere. This material showed good activities toward ORR. However, these methods contain the preparation of hard template and the followed removing process of the template, which make the preparation method complicated. Moreover, the washing process can easily introduce the O-containing functional, which can cause the decrease of the catalytic activity for the catalysts. In our previous work, we have developed a simple soft-template strategy synthesizing nitrogen-doped porous carbon electrocatalysts with the PANI as precursor.[15] The resultant catalyst exhibits a comparable electrocatalytic activity and better stability during ORR in alkaline fuel cells than a commercial Pt/ C catalyst. Moreover, we have found that the pyrolysis temperature plays a crucial role in the catalytic activity of the electrocatalysts. However, it is still ambiguous about the active sites and how the pyrolysis temperature affects the catalytic activity. Moreover, there is no report about the PNCEs with the graphene-like amorphology and hierarchically porous structure derived of polyaniline and polyvinylpyrrolidone composites acting as ORR and poison-tolerant electrocatalyst in acid electrolyte PEFCs.

Furthermore, the active sites and the nature of the formation of active sites for ORR on nitrogen-doped carbon catalysts are still under discussion. Especially, the role of the transitional metal is still in controversy. Some researchers believed that the transition metals remained in the carbon-based catalyst after acid washing might work as an active site[16, 17]. However, some researchers believe that the transition metal does not act as an active reaction site for oxygen reduction, but rather serves primarily to facilitate the incorporation of nitrogen into the graphitic structure and to form doped carbon materials with higher amounts of edge plane exposure, which is more active for ORR [18, 19]. Thus, it is necessary to make great efforts for extensively clarifying the catalytic sites of the nitrogen-doped carbon.

In this paper, we synthesized the nitrogen-doped carbon catalysts by chemical polymerization of aniline monomers with polyvinylpyrrolidone (PVP) as soft template and stabilizing reagent, followed by pyrolyzing the composite under higher temperatures. The catalyst presents grapheme-like structure and hierarchical pore distribution. The ORR catalytic activity and catalytic mechanism of ORR in PEFCs with acid electrolyte have been investigated. The role of the PVP will also be discussed. Furthermore, it was proved that the etching effect of NH_3 under high temperature during the carbon synthesis can significantly change the structure of the carbon materials[20]. Thus, the effect of the pyrolysis temperatures and gas atmosphere on the pore structure, nitrogen species and nitrogen contents as well as the catalytic activity for ORR has been explored. X-ray photoelectron spectroscopy (XPS) of Fe was used to investigate the Fe oxidation state and X-ray absorption near-edge structures (XANES) of Fe were applied to determine the oxidation state and chemical speciation of iron. The results demonstrate that the catalysts display high catalytic activity, excellent methanol and SO_2 tolerance and superior stability in acid medium. The PNCEs prepared at 1000 ^oC achieving a maximum power density of 456 mW cm^{-2}, exhibits the best catalytic activity toward ORR compared with the catalysts pyrolyzed at 700 ^oC, 800 ^oC, 900 ^oC, and 1100^oC. It also reveals that it is not the nitrogen content, but the nitrogen bonding configurations, textural structure, and pore structure of PNCE play key roles in the electrocatalytic activity towards the ORR. This is the first time that the nitrogen-doped carbon derived from the PANI-PVP is reported to act as both the main active component and poison-tolerant components for ORR catalysts in acid electrolyte PEFCs. The PNCEs brings us a promising alternative of Pt-based precious catalysts.

Experimental

Catalysts Synthesis

The PNCE were synthesized by chemical polymerization of aniline (A) with PVP followed by heat-treatment in the presence of ammonia according to our previous work.[15] Fe $(NO_3)_3$•$6H_2O$ was added after the polymerization immobilized homogeneously throughout the pores of the PANI-PVP. As shown in the scheme 1, the PANI colloids were firstly synthesized by polymerization of aniline and PVP using ammonium persulfate ($NH_4S_2O_8$) as oxidant at room temperature: First, 10 mL fresh aniline hydrochloride aqueous solution containing 2.5 mL aniline, 1.5 mL hydrochloride (37 wt%) and 2.5 g of polyvinylpyrrolidone (PVP K30) were added into the mixture of ethanol and water (volume ratio of 5:1), followed by stirring for about 30 min. Secondly, 25 mL of 0.1 M $NH_4S_2O_8$ aqueous solution was added dropwise, as oxidant and initiator. When the mixtures completely turned green by keeping stir for 3 h, the Fe $(NO_3)_3$•$6H_2O$ (M), was added with the A: M mol ratio of 1/20, respectively. After stirring for 24 h, the obtained green products were dried in a water bath at 70 ^oC and in vacuum oven for 48 h to obtain the PANI-M-PVP composites. Thirdly, the composites were cut by the muller, which was different with our previous work.[15] Fourthly, the composites were transferred to the tube oven for pyrolysis under flowing NH_3 or N_2 atmosphere at a flow rate of 100 mL min^{-1}. The temperature was first increased to 300^oC at a rate of 1.5 ^oC min^{-1}, then to 500 ^oC at a rate of 5 ^oC min^{-1}, and finally to the reaction temperatures at 1.5 ^oC min^{-1} followed by maintaining at the reaction temperatures for 2 h. Finally, the catalysts were ball-milling for 5 h at a rotating rate of 400 rpm. The catalysts heat-treated at 700 ^oC, 800 ^oC, 900 ^oC, 1000 ^oC and 1100 ^oC with Fe species under NH_3 were recorded as PNCEs-700, PNCEs-800, PNCEs-900, PNCEs-1000, and PNCEs-1100, respectively. The catalyst synthesized without PVP at 1000 ^oC under NH_3 was noted as NNCEs-1000. The PANI-N_2 catalysts (PNCEs-N_2) pyrolyzed under N_2 atmosphere was also prepared as comparison, respectively.

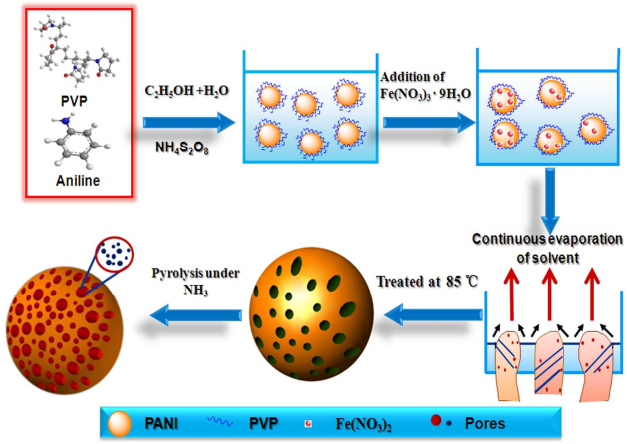

Scheme 1. Schematic illustration of the synthesis process for the PNCEs

Physical Characterizations

X-ray diffraction (XRD) analyses of the catalysts were carried out on a Dandong Haoyuan Instrument Co., LTD) using Cu-Kα radiation (λ = 1.54056 Å) operating at 40 kV and 40 mA. The 2θ values of X-ray diffractograms varied between 30° and 85°.

Transmission electron microscopy (TEM) images were recorded on a FEI Tecnai G2 microscope with 120 kV accelerating voltage. Sample for TEM measurement was prepared by ultrasonically suspending catalyst powder in ethanol and then placing a drop of the suspension to a holey amorphous carbon film on a Cu grid.

A thermo VG ESCALAB250 spectrometer with a monochromatic Al K□ source (1486.6 eV, 15 kV, 250 W) was applied to measure the X-ray photoelectron spectroscopy (XPS) spectra. The XPS energy scale was calibrated by setting the binding energy of the carbon support to exactly 284.6 eV referenced to the Fermi level. Deconvolutions of the XPS spectra were carried out using software XPS peak fit 4.0. Relative concentrations of the surface species are equal to the corresponding deconvoluted peak areas divided by the total XPS signal area extracted from the experimental XPS core level regions of N1s.

Raman spectra of dried samples were obtained on Renishaw invia Raman Microscope with excitation by an argon ion laser (514 nm) to determine the defects and structures of the as-prepared carbon materials.

N_2 adsorption–desorption at 77.3 K were collected on an ASAP2010 volumetric adsorption analyzer (Micromeritics Instrument Corporation, USA) to characterize the surface area and pore structure of the catalysts. The samples were degassed at 100°C for 10 h under vacuum before the test. The specific surface area was determined according to the Brunauer–Emmett–Teller (BET) method in the relative pressure range of 0.05–0.2. The pore size distribution (PSD) was determined by the desorption data.

The X-ray absorption near-edge spectra (XANES) were collected on Beijing Synchrotron Radiation Facility, BSRF. The XANES spectra of the samples and references were measured in the fluorescence-detection and transmission modes at room temperature, respectively. The Fe k-edge regions of the spectra were utilized to determine the oxidation state and chemical speciation of iron by the comparison with the XANES region of iron containing standards using linear combination fitting of the Athena software. Referred to the results of Wu et al. [21], we have chosen the Fe-containing standards including (1)1,10-phenanthroline with iron(II) sulfate complex are grouped under pyridinic $Fe–N_{2+2+2}$. (2) 5,10,15,20-tetrakis(4-sulfonatophenyl)-21H,23H-porphine iron(III) chloride (FeTPPS) (16456-81-8), which are grouped underpyrrolic $Fe–N_4$ (3) Iron(II) phthalocyanine and chloroproporphyrin (Iron (III), which are grouped underporphyrazin $Fe–N_4$. (4) FeS (5) Fe_2N.

Electrochemical measurements

A VMP3 potentiostat (Biologic Instrument) electrochemical analyzer and a RDE glass cell were used for electrochemical measurements. The counter electrode was a Pt wire, and the reference electrode was an Hg_2Cl_2/Hg/saturated KCl electrode, which was 0.242 V vs. standard hydrogen electrode (SHE). The thin-film coated glassy carbon electrode (GCE) served as the working electrode and the electrolyte was aqueous 0.5 M H_2SO_4, respectively. All potentials were referred to SHE and all electrochemical data were obtained at room temperature.

The catalyst ink for the working electrode was prepared by using the method described in our previous work[20]: briefly, 5 mg catalyst was dispersed ultrasonically in a mixture containing 1 mL isopropyl alcohol and 50 mL Nafion (5 wt% solution, DuPont). The modified GCE was loaded with as-prepared catalysts or 20 % JM-Pt/C, followed by drying at room temperature for 2 h. The electrolyte solutions were purged with high-purity N_2 gas for about 1 h before tests. Before recording, the potential was repeatedly scanned 10 cycles to remove any residual impurities. Then, the 0.5 M H_2SO_4 electrolyte was saturated with oxygen by purging O_2 for at least 30 min. The polarization curves for ORR were obtained in O_2-saturated 0.5 M H_2SO_4 at rotation rate of 1600 rpm. The scan rate was fixed at 5 mV s^{-1}.

A modified rotating glassy carbon disk (diameter 5.61 mm) - platinum ring electrode (0.1867 cm^2) （RRDE）was used as working electrode to test the H_2O_2 production rate. The collection efficiency (N) of the ring electrode obtained by reducing ferricyanide at the disk electrode was 0.37. The fabrication of catalysts ink for RRDE is the same with that of RDE test. Before the RRDE experiments, 20 μL of catalyst ink was coated onto the glassy carbon electrode, and oxygen gas was saturated in the electrolyte by bubbling the gas for 30 min.

Accelerated aging tests were carried out to evaluate the stability of electrocatalyst towards the ORR. The experiments were performed by the potential scanning accelerated aging test (AAT) between 1.04 V-0 V vs. SHE for 1000 cycles in nitrogen-saturated 0.5 M H_2SO_4 (50 mV s^{-1}). Before and after the AAT, the ORR polarization curves were recorded to evaluate the stability of the catalyst.

Methanol Tolerance measurements

Methanol tolerance measurements were carried out in O_2-saturated 0.5 M H_2SO_4 solution containing 0.5 M methanol. The polarization curves for ORR were collected at the scan rate of 5 mV s^{-1}. The 20% Pt/C (Jonson Matthey Com.) was chosen as the comparison.

SO_2 Tolerance Evaluations

The evaluations of the SO_2 tolerance for the catalysts were conducted by the method described in the references [5]. Firstly, the electrolyte for sulfur dioxide tolerance measurement was prepared by introducing 0.1 M anhydrous Na_2SO_3 into 0.5 M H_2SO_4. The Na_2SO_3 reached equilibrium between SO_3^{2-} and SO_2 in the acid electrolyte and the concentration of the poison species was calculated on the basis of the total amount of S (IV) initially dissolved. Saturated with ultra-pure N_2, the PNCEs and 20% Pt/C catalysts were poisoned by holding the GCE at the potential of 0.65 V in the 0.1 M Na_2SO_3/0.5 M H_2SO_4 for 2 min. Then the electrodes were withdrawn covered with a droplet of this solution and rinsed with more than 100 mL deionized water. Subsequently, the electrode was introduced into a clean 0.5 M H_2SO_4 electrolyte saturated with oxygen and the ORR polarization curves of the SO_2 poisoned electrodes were recorded at a sweep rate of 5 mV s^{-1} from 1.042 V to 0.0 V at a rotating speed of 1600 rpm. The ORR polarization curves with and without SO_2 were compared to evaluate the SO_2 tolerance of the catalysts.

Fabrication of Membrane Electrode Assembly and Single Cell Test

The membrane electrode assembly (MEA) used in single cell tests was prepared with PNCEs-1000 as the cathode electrocatalyst. The area of the electrode was 5 cm^2. The 46.7 wt. % Pt/C catalyst (TKK) was used as the anode catalyst with the Pt loading of 0.3 mg cm^{-2} and the Nafion®-212 (Du Pont) was used as the membrane. The cathode was prepared as follows: the catalysts were mixed with appropriate amount of isopropanol and 5% Nafion® solution suspension (PNCE: Nafion = 2:1 by dried weight) and ultrasonicated to form an ink-like slurry; the slurry was then cast onto a prefabricated gas diffusion layer (Toray carbon paper as substrate, 30 wt. % PTFE) and heat-treated at 130 ^oC for 30 min in a vacuum oven to obtain the cathode electrode. The cathode catalyst loading is about 3.0 mg cm^{-2}. The MEA was fabricated as follows: the membranes were sandwiched between two gas diffusion layers followed by a hot-pressing procedure at 140 ^oC, 1MPa for 1 min and 10 MPa for 1 min to fabricate the membrane electrode assembly (MEA). Fuel cell polarization curves (I-V) measurement was carried out at the cell operating temperature of 80 ^oC. The fuel (H_2) and the oxidant (O_2) were humidified by passing them through humidifier at temperatures of 90 ^oC and 85 ^oC, respectively. The gas pressures were all kept at 0.2 MPa at both electrodes. Performance data were recorded in the steady state and the polarization curves were uncorrected for internal resistance losses. Then I-V curves of the cells were tested in galvanostatic mode.

Results and discussion

Scheme 1 illustrates the synthesis process of the PNCEs. The PANI was obtained by the aniline polymerization process with the ammonium persulfate ($NH_4S_2O_8$) as the initiator. Ball-like polymers well dispersed in the solvent, were formed with the PVP acting as the template and pore former. The aqueous Fe salt was then added into the mixture. Additionally, after the continuous evaporation of the solvents, the polymers with porous structure can be obtained. Finally, the pyrolysis process under NH_3 atmosphere at high temperature contributes the further change of the textual structure and pore structures.

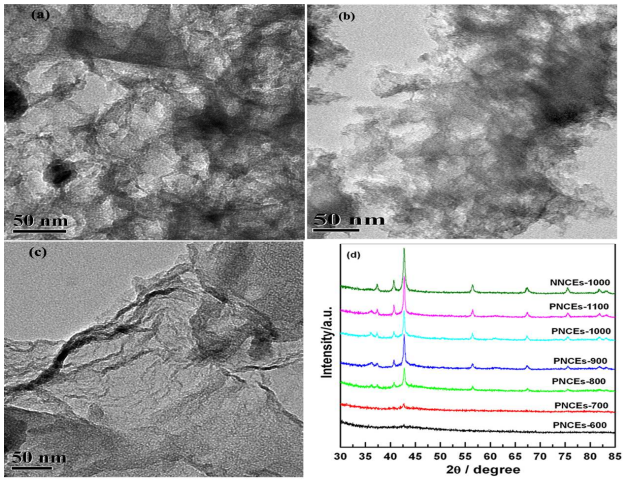

Fig.1 TEM images for the (a) PNCEs-700 (b) PNCEs-1000 (c) NNCEs-1000 (d) XRD patterns for different catalysts.

Transmission electron microscope (TEM) images were used to characterize the morphology of the catalysts. Fig. 1 shows the TEM images of the as-prepared PNCEs-700, PNCEs-1000, and NNCEs-1000. It reveals the NNCE-1000 catalyst presents morphology similar to graphene-sheet structure (shown in Fig. 1c)[22]. Comparatively, the skeleton of the PNCEs-1000 consists of interconnected, spongy and porous structure partly maintaining graphene-sheet structure. That proves the addition of PVP into the aniline during the polymerization can significantly change the structure of the as-prepared carbon catalysts and partly break the graphene-sheet structure, forming more pores in the carbon framework. The PVP acts as the stabilizer and disperser, which can hamper the agglomeration of the PANI and obtain uniformly, dispersed PANI balls. Moreover, the PVP can also promote the formation of new pores, which contributes the improvement of the porosity for the PNCEs. Fig.1c gives the TEM images of PNCEs-700. It is obvious the morphology of the PNCEs-700, which presents spongy and porous structure, shows lower porosity than that of PNCEs-1000.

The XRD spectra were collected to characterize the structure of the catalysts. Fig. 1d shows the XRD patterns of PNCEs prepared at different temperatures and NNCEs. For the PNCE-700, the XRD pattern presents diffraction peaks at 42.7°, which are attributed to iron nitride (Fe_2N) (011) (PDF card: 01-072-2126). No obvious peaks correspond to the characteristic peaks of iron oxides and iron. When the pyrolysis temperature increases to 800^oC, the peaks at ca. 40.8°, 42.9°, 37.5°, 56.6°,67.5°,75.8° and 82.1° appear, which are attributed to the diffraction peaks of Fe_2N (PDF card: 01-072-2126). Moreover, with the increase of the

pyrolysis temperature, the peaks corresponding to the Fe nitrides become sharper, which demonstrates the increase of the Fe_2N particles size. No obvious peaks corresponding to metallic Fe (44.8° and 64.2°) and Fe_3O_4 (41.9°, 56.3° and 63.1°) as well as FeS can be observed, which may be attributed to the nitrification of Fe species under NH_3.[22] The XRD pattern of NNCE-1000 is similar to that PNCEs-1000 except the characteristic peaks for Fe_2N are sharper. That indicates the particles size of Fe_2N is smaller for PNCEs, which proves the addition of PVP can partly decrease the particles size of the metal species.

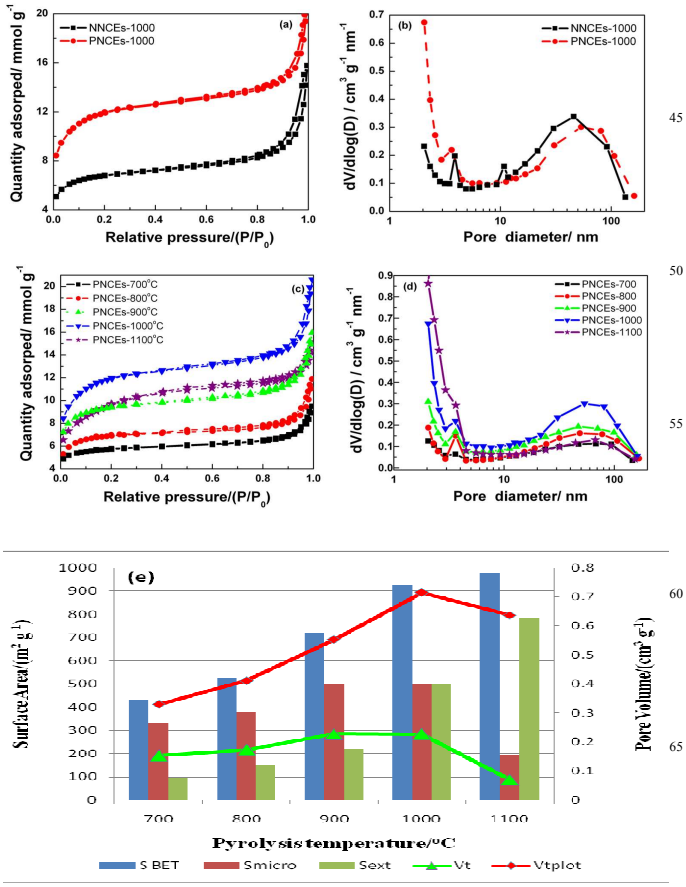

Fig.2 (a), (c)Typical N_2 sorption isotherms of the resultant nanoporous carbon catalysts; (b), (d) their corresponding BJH PSDs and (e) pore structures of different catalysts.

The nitrogen-absorption measurements were performed to investigate the specific surface area and the pore structure. Fig. 2 shows the N_2 sorption isotherms and the corresponding pore size distribution (PSDs) of the as-synthesized carbon catalysts. As shown in Fig. 2a, compared with the NNCEs-1000, the PNCEs-1000 displays higher surface area and pore volume. This further proves the addition of PVP creates more pores for the carbon, which improves its surface area and pore volume. Fig. 2c gives the N_2 sorption isotherms of the PNCEs synthesized under different temperature. The results demonstrate that the pyrolysis temperatures of the PNCEs can significantly change their pore structures. It is also evident that the isotherm plots of PNCEs is type IV with a hysteresis loop over the whole relative pressure range, indicating the presence of abundant pore in the carbon spheres. A rise below the relative pressure of about 0.1 can be attributed to the adsorption on microporous carbon layers.[8,23] When pyrolysis process is carried out at 700°C, the PNCEs-700 shows the lowest nitrogen uptake, which corresponds to less-developed porosity. The increase of the pyrolysis temperature leads to a significant increase in nitrogen uptake, indicating well developed porosity. Table S1 present the pore structure properties of the catalysts. It is clear that with the increase pyrolysis temperature, the BET surface area gradually increases from 432.7 $m^2\ g^{-1}$ for PNCEs-700 to 924.6 $m^2\ g^{-1}$ for PNCEs-1000 and decreases to 756.6 $m^2\ g^{-1}$ for PNCEs-1100. Moreover, the pore volume improves significantly (0.329 cm^3/g for PNCEs-700 to 0.715 cm^3/g for PNCEs-1000), followed by a decrease to 0.518 cm^3/g for PNCEs-1100. The decomposition of the polymer as well as the etching reaction between the NH_3 and carbon contributes to the increase of the surface area and the pore volume.[24] Fig.S1 exhibits the corresponding pore size distribution (PSD) of the PNCEs synthesized under NH_3 and PNCEs-N_2 catalysts. The difference in pore structures further proves that the reactions between carbon and NH_3 involving the replacement of oxygen-bearing species by nitrogen-containing groups and the etching of carbon fragments by the radicals generated by the decomposition of NH_3 at high temperatures. This forms more pores including the micropore and mesopore as well as macropores. However, the pyrolysis under 1100°C can cause the collapse of some macropores, which may result in the decrease of the surface area.

The PSD curves were calculated to study the pore structures in the range of 2-300 nm. As shown in Fig. 2b and Fig.2d, the resultant PNCEs and PNCEs catalysts all have hierarchical pore structures containing both macroporous and mesoporous pores as well as micropores in the carbon framework. From Fig. 2b, the PSD of NNCEs-1000 is different from that of PNCEs-1000, with less macropore, mesopore and micropores. Moreover, the pore size of macropores of PNCEs-1000 is a little larger than NNCEs and the peaks for micropores increases sharply, which suggests that the PVP has enlarged the pores sizes and created more mesopores as well as micropores.

As shown in Fig. 2d, it also demonstrates that the carbonization temperature plays a critical role in the pore structure of the resulting catalysts. With the increase of the pyrolysis temperature, the pore distribution peaks for the mesopores gradually become sharp. Moreover, the absorbed gas volume at low relative pressure below 0.1 increases with the further improvement of temperature demonstrating the increase of microspores. From Table S1, it is clear the contribution of micropore to the total surface area and pore volume enhances as the treatment temperature increases to 1000°C, while decreases for the PNCEs-1100. Furthermore, the macropore peaks gradually become shaper when the temperature increases from 700°C to 1000°C. However, it turns to be less sharp for the PNCEs-1100. Apparently, the PNCEs-1000 presents the highest micropore surface area and pore volume. This should be attributed to the etching effect of NH_3 and the decomposition of precursors at higher temperature. It can also be seen that the PNCEs-1100 presents decreased mesopores as well as macropores, compared with that of NNCEs-1000. This suggests some macropore collapse and micropore enlargement under the high temperature

and NH_3 etching atmosphere may result in its loss of surface area and the decrease of the pore volume. [25]

Raman spectra were collected to characterize the carbon structure and disorder degree. Fig.3a gives the Raman spectra of the PNCEs catalysts synthesized at different temperatures. The G-band peak at about 1595 cm^{-1} and the D band peak at about 1365 cm^{-1} can be observed. The D-band is associated with the defects, curved sheets and dangling bonds in the carbon structures, while the G-band corresponds to the graphitic carbon with a sp2 electronic configuration. The intensity of the D mode is typically normalized with respect to the intensity of the G mode (I_D/I_G ratio) for estimating the defect concentration. With the increase of the pyrolysis temperature, the I_D/I_G gradually decreases, which demonstrates the higher degree of graphitization at higher temperature. The 2D-band corresponds to the graphene or the graphite with a high degree of graphitization. [26] It is clear that a broad 2D-band at about 2697 cm^{-1} appears in the spectrum when the pyrolysis temperature increases to 900°C, which becomes sharp for PNCEs-1000 and PNCEs-1100. The phenomenon is in accordance with the results reported in reference. [27,28]

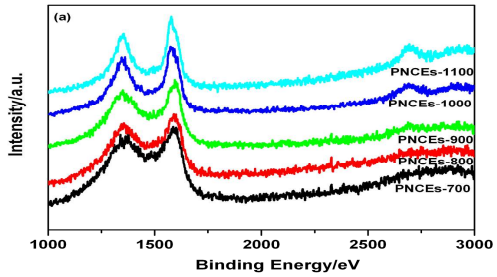

Fig. 3 Raman spectra

X-ray photoelectron spectroscopy (XPS) measurements were conducted to elucidate the surface chemical compositions and the nitrogen configurations of the catalysts. Fig. 4 demonstrates that the chemical composition of the different catalysts is significant different. It is clear the increase of the pyrolysis temperature leads to the decrease in nitrogen content from a maximum 3.68 at% at 700°C to 0.48 at.% at 1100 °C. This may be attributed to the break of nitrogen-carbon bond, which is caused by the attack of NH_3 toward the polymer structure during the pyrolysis process.

Nitrogen can be present in different forms nitrogen doped carbon including pyridinic-N, pyrrolic-N, quaternary-N, and pyridine-N-oxide. Fig. 4a-4f shows the deconvoluted XPS spectra of N1s of different catalysts. Five different types of nitrogen atoms with different binding energies can be deconvoluted with the XPS 4.1 software. Pyridinic-N (398.1 eV±0.2, N1) is a type of nitrogen that contributes one p-electron to the π-system and has a lone electron pair in the plane of the carbon matrix, which can increase the electron-donor property of the catalyst[20,21]. The pyrrolic-N (399.8 eV±0.2, N2), refers to the N atoms bonded with two carbon atoms, which is incorporated into five member heterocyclic rings and contributes two p electrons to the π system. Quaternary-N (401.0 eV, N3) is the graphitic nitrogen in the center of heterocyclic rings, which locates in the perfect graphite plane by bonding with three carbon atoms. Pyridine-N-oxide (403.5±0.2 eV, N5) refers to N atom bonded with two carbon atoms and one oxygen atom. For the peak at 401.9 eV±0.2 eV, some researchers believed that it was contributed to the pyridine-N-oxide [29] and some thought it reflected the presence of graphitic-N at the valley, which located at the edge of the heterocyclic rings.[22, 30] It was reported that the nitrogen oxide functionalities exhibited low thermal stability.[29] From our results, the ratio of N4 increases with the increase of the pyrolysis temperature. Therefore, this peak in this article should be assigned to graphitic nitrogen, which is in agreement with the observations of Sharifi et al.[30]

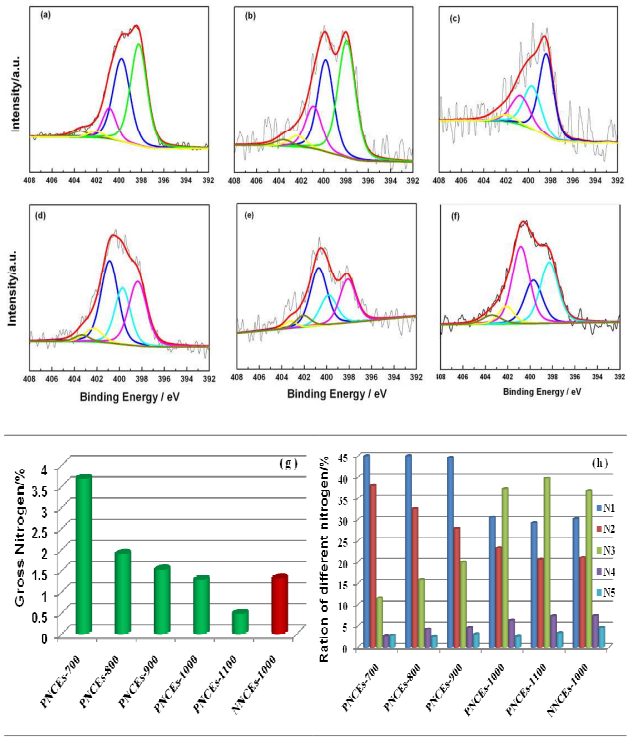

Fig. 4 XPS spectra of N1s (a) PNCEs-700 (b) PNCEs-800(c) PNCEs-900(d) PNCEs-1000 (e) PNCEs-1100 and (f) NNCEs-1000 catalyst (g) Gross nitrogen-content of different catalysts (h)Nitrogen configurations for different catalysts

As shown in Fig. 4g, it can be observed that with the increase of the pyrolysis temperature, the nitrogen configuration changes significantly. The N1 content changes little at the pyrolysis temperature lower than 900 °C, while gradually decreases as the temperature increases to 1000°C. Furthermore, the N2 quickly decreases when the pyrolysis temperature increases from 700°C to 1100°C, which indicates that the N1 is more stable than N2. Comparatively, the N3 and N4 ratios increase with the improvement of the pyrolysis temperature. The gradual transformation of N1 and N2 to graphitic nitrogen (N3 and N4) may contributes to the significant change of nitrogen configurations for the catalysts synthesized at different temperature.[30] Compared with the PNCEs-1000, the NNCEs-1000 presents similar nitrogen configuration except the higher N5 content. The higher N5 content of the NNCEs-1000 maybe correlate its higher graphitic structure.

From the XPS, the surface Fe content of PNCEs-1000 and NNCEs-1000 are 0.21 at. % and 0.26 at. %, respectively. Figure S2 shows the Fe 2p spectrum of PNCEs-1000 and NNCEs-1000. As shown in Fig. S2, it can be deconvoluted into five peaks at 710.4, 713.4, 718.1, 722.9, and 725.4 eV for the two catalysts. The peak at 725.2 eV corresponds to the binding energies of 2p1/2 of Fe(III) ion and the peaks at 722.9 eV can be assigned to the binding energies of 2p 1/2 of Fe(II) ion. The peak at 713.6 eV and 710.7 eV can be assigned to the 2p3/2 of Fe (III) ion and Fe (II) ion, respectively. The peak at 718.7 eV is a satellite peak of Fe^{3+} 2p1/2. This result suggests the co-existing of Fe(II) and Fe(III) in the catalysts. [31,32] However, we cannot obtain the exact species in the catalysts from the results. Thus, the metallic states of the iron species in the PNCEs-1000 and NNCEs-1000 are further investigated by X-ray absorption near-edge spectra (XANES) of Fe K-edge (Fig. S3a), which is sensitive to the chemical state of atoms. The XANES spectra demonstrate that the Fe environment in PNCEs and NNCE is significantly different from FeS, suggesting that the absence of FeS in the NNCEs-1000 and PNCEs-1000. Fig.S3b shows the Fourier-transformed magnitudes of k3-weighted Fe K-edge EXAFS of different catalysts and reference samples. The Fe environment around Fe is different. The coordination environment around Fe in NNCEs is similar to that of the Fe_2N. This indicates the ligand of the Fe-N formed for the NNCEs, which is in agreement with the results of XRD. However, the coordination environment around Fe of PNCEs is different with that of the NNCEs. Combining XANES linear summation and EXAFS analysis, the coordination number of the central iron atom is nearly 4. Both porphyrazin Fe–N_4 and underpyrrolic Fe–N_4 are found in PNCEs. Although the existence of Fe_2N in PNCEs, the ratio of the Fe_2N in PNCEs is lower than that of the NNCEs. The existence of Fe_2N is also detected by XRD (Figure 1c). This can be explained that the addition of PVP can improve the ratio of micropores, which may consequently promote the formation of the FeN_x in the micropores. Comparatively, the NNCEs-1000 presents sheet-like morphology with low porosity and micropores, which may contribute to the higher ratio of Fe_2N and low content of FeN_4. No iron sulfide species can be detected by XANES for the catalysts, which agrees with the results of XRD.

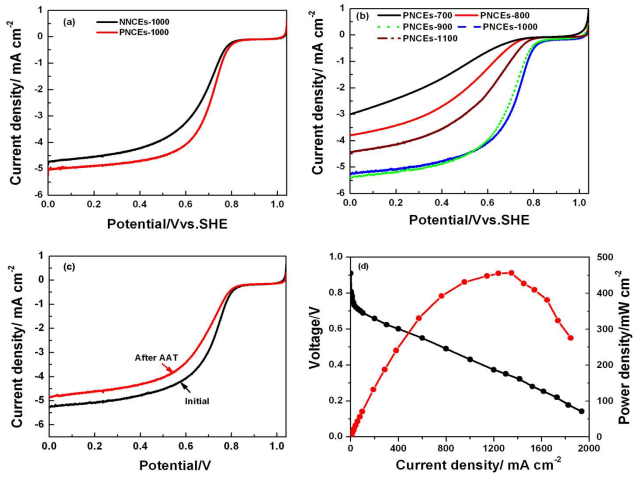

Fig. 5 (a) Oxygen reduction polarization curves for the catalysts PNCEs-1000 and NNCEs-1000 O_2-purged 0.5 M H_2SO_4; (b) ORR polarization curves on PNCEs synthesized at different temperature. (c) Polarization curves before and after AAT for ORR. Rotating rate is 1600 rpm. Scan rate=5 mV s^{-1}. (d) Performance of the single cell with PNCEs-1000 as the cathode catalyst. The catalyst loadings of the cathode is 3.0 mg cm^{-2}; Anode humidifier temperature: 90 ^oC; Cathode humidifier temperature: 85 ^oC; Pressure: 0.2MPa/0.2MPa; Cell operating temperature: 80 ^oC.

In order to study the ORR activity, the polarization curves were collected in O_2-saturated 0.5 M H_2SO_4 at room temperature. Fig. 5a shows the ORR polarization curves for PNCEs-1000 and NNCEs-1000 catalysts. It can be observed that the ORR curves for PNCEs-1000 is obviously positive than that of NNCEs-1000, which further proves the improvement of catalytic activity with the addition of PVP during the synthesis process of the catalysts. According to the results from XPS and nitrogen adsorption in the Fig.4 and Fig. 2, compared with the NNCEs-1000, the PNCEs-1000 has higher surface area, pore volume and higher graphitic nitrogen species, which maybe contribute its higher catalytic activity. The difference of Fe species may also cause their difference of the catalytic activity. Fig.5b shows the ORR polarization curves for PNCEs-T catalysts synthesized at different temperatures. The PNCEs-700 shows lowest catalytic activity for the ORR. The potentials at current density of 1 mA cm^{-2} for PNCEs-700, PNCEs-800, PNCEs-900, PNCEs-1000, PNCEs-1100 are 0.524 V, 0.628 V, 0.760 V, 0.773 V, 0.697 V vs. SHE, respectively. It suggests that the ORR activity enhances at elevated synthesis temperature and the best activity is achieved for PNCEs-1000 with an onset potential of 0.90 V. From Fig.S4, the half-wave potential between the PANI-1000 and 20% Pt/C is smaller than 100 mV, which demonstrates the possibility of its application as ORR catalyst. From Fig.4g, it is clear the nitrogen content in the PNCEs is largely decreased with the increase of the pyrolyzed temperature from 700 to 1100^{o}C. From Fig. 2e and Fig. 4 h, the PNCEs-1000 shows the highest surface area and contains a very low nitrogen species. Comparatively, the PNCE-700 exhibits the lowest surface area and highest nitrogen content. It has been proved that the introduction of nitrogen doping is necessary for the improvement of ORR activity on carbon, due to the enhanced electron donating ability and electron density resulting from the valence electrons donated by the nitrogen. [34] However, the results demonstrate that gross nitrogen content in PNCEs does not play a key role in their catalytic activity, which is consistent with our previous work. [20]

With the improvement of the pyrolysis temperature, the total surface area and micropore surface increase and the ratio of micropores is also improved. Among the catalysts, the PNCEs-1000 presents the highest micropore surface area and micropore volume. Jaouen et al. [16]has demonstrated that the proposed active sites for ORR, Fe-coordinated nitrogen compounds such as FeN_2 and FeN_4, were hosted in the micropores. From our results of XPS and XANES, we have proved the existence of FeN_x and the CN_x species in our catalysts, which may be located in the

micropore and works as the active sites. Moreover, the hierarchical pore structure composed of macropores pores, mesopores and micropores of the PNCEs may also benefit for the high performance of the catalysts for PEFCs.[35] The micropores and mesopore in the unique architecture can confine the active sites for ORR, while the macropores as well as mesopores are more easily accessible to gaseous molecules and can transport reactants to the surface of the active sites, which contributes the high activity for the catalysts. [36]

The role of the different nitrogen species on the ORR activity is still in debate. Ozkan and his group [37] proposed that the pyridine-like nitrogen and graphite-like nitrogen acted as the active sites of the graphitic nitrogen-doped carbon. They insisted that the catalysts with a relatively larger amount of pyridine-like nitrogen exhibited a higher ORR activity than those with a relatively larger amount of graphite-like nitrogen. But some researchers considered the quaternary-N as ORR catalytic sites both experimentally and theoretically due to the reduced adsorption energy.[38,39] Furthermore, the quaternary-N was considered more stable than pyridinic-N in acid media. [30] From our results, it can be observed with the increase of the pyrolysis temperature, the N3 content increases, while N2 and N1 content decreases combining with the improvement of the catalytic activity. That means the catalytic activity of the catalysts does not correlate directly with the content N1 and N2. With the increase of pyrolysis temperature, the N3 and N4 contents increase gradually and the catalytic activity of the catalysts improves, which suggests that the N3 and N4 may contribute to the higher ORR activity of PNCEs-1000. However, when the temperature increases to 1100°C, the N3 and N4 content achieves the highest value, while its surface area decreases and pore structure changes, which may consequently induce its catalytic activity decrease. Furthermore, although the PNCEs and NNCEs contains similar N3 amount and the NNCEs presents higher N4 content, their performances for ORR are greatly different. That means that the N3 and N4 content is not the only factor deciding the ORR activity although they contribute the high activity of PNCEs. The performance of the different catalysts should be the combining role of the nitrogen configuration, pore structure and transition metal species.

The Fe_2N has been proved to be effective for the ORR [40]. From the XRD, the particle sizes of the Fe_2N increase with the increase of the pyrolysis temperatures, which should results in the decrease of active area and the catalytic activity. This further demonstrates that Fe_2N is not the main active sites of the PNCEs. From our results of XANEs, we can find that both the PNCEs and NNCEs contain the FeN_x species and NNCEs presents lower FeN_x ratio than PNCEs. Moreover, the catalyst with higher catalytic activity presents higher micropores surface area in the carbon framework. That means only the FeN_x hosted in the micropores may acts as the active components.

To further evaluate the catalytic activity of the PNCEs-1000, curves of the cell voltage and power density against current density were recorded at cell operating temperature of 80 °C in H_2/O_2 PEMFC under 0.2 MPa pressure. Fig.5d shows the performances of the single cell with the as-prepared PNCEs-1000 as the cathode electrocatalyst. As illustrated in Fig.5d, the catalyst exhibits high activity toward the ORR. At the current density of 200 mA cm^{-2}, the cell voltage of the single cell is 0.658 V. The maximum power density, W_{max}, about 456 mW cm^{-2}, is achieved at 1416 mA cm^{-2}. This further demonstrates the high catalytic activity of the PNCE-1000.

Fig.5c presents the ORR curves before and after cycling performance of PNCEs-1000. Apparently, the PNCEs-1000 exhibits an excellent stability within 1000 cycles. It can retain 69.5 % of initial current density at 0.7 V, which is higher than that of 20 Pt/C (32.3% retention) reported in our previous work because of its excellent stability. [20] The higher stability of the PNCEs-1000 in 0.5 M H_2SO_4 may be attributed to the high graphitic degree and the strong C-N bond as well as the absence of degradation caused by the Pt metal.

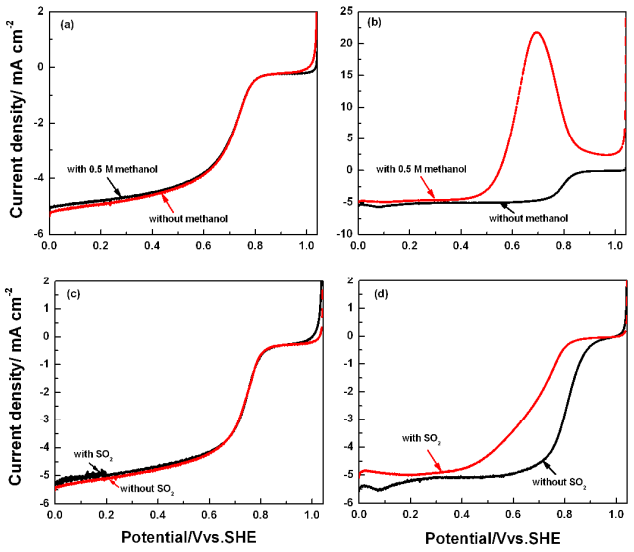

Fig. 6 Polarization curves for ORR of nitrogen-doped carbon catalysts in O_2-purged 0.5 M H_2SO_4 solution with and without 0.5 M methanol (a) PNCEs-1000; (b) 20% Pt/C; ORR curves in O_2-purged 0.5 M H_2SO_4 solution with and without SO_2 of (c) PNCEs-1000; (d) 20% Pt/C; Scan rate: 5 mV s^{-1}. Rotation rate: 1600 rpm.

To investigate the methanol tolerance of the PNCEs, the cathode polarization curves of the PNCEs-1000 was collected in the 0.5 H_2SO_4 with and without 0.5 M methanol. As shown in Fig. 6, a significant anodic peak is present for the 20% Pt/C during the reduction sweep from 1.04 V to 0 V in 0.5 H_2SO_4 with 0.5 M methanol, which is attributed to the oxidation of methanol. The great losses of catalytic activity in 0.5 H_2SO_4 with 0.5 M methanol for the Pt/C are caused by the mixed potentials from methanol on the cathode. [41] However, except a small decrease in the limit current, almost no change occurs on the polarization curves for the PNCEs-1000. This confirms that the PNCEs is tolerant to methanol and does not experience the mixed potentials that occur with platinum catalysts.

The SO_2 tolerances of the PNCEs-1000 and 20%Pt/C were evaluated by poisoning the electrodes in N_2-sataurated 0.5 M H_2SO_4/0.1 M Na_2SO_3 for 2 min at 0.65 V. The Na_2SO_3 reached

equilibrium between SO_3^{2-} and SO_2 in the acid electrolyte and the SO_2 adsorption was formed on catalysts. Fig. 6c shows the ORR polarization curves of PNCEs-1000 before and after SO_2 poison. It is clear the potentials no obvious shift and no obvious change occurs for the limit current density. However, the half-wave potential of the Pt/C significantly decreases from about 0.81 V to 0.68 V (Fig. 6d). Moreover, the ORR limiting current also decreases, which may be attributed to the part coverage of Pt surfaces by sulfur compounds. [5] This result prove that the PNCE-1000 presents superior SO_2 tolerance compared with JM-20% Pt/C, which may be ascribed to the weak adsorption of SO_2 on the surface of PNCE-1000.

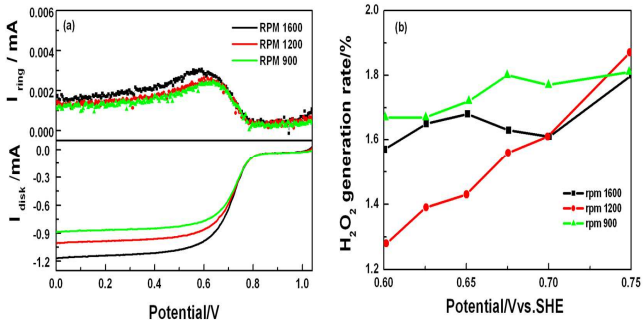

Fig. 7 RRDE curves (a) and H_2O_2 production rate (b) for ORR of PNCEs-1000 in O_2-purged 0.5 M H_2SO_4 solution. Scan rate: 5 mV s^{-1}. Rotation rates are indicated in the graph; sweep rate 5 mV s^{-1}; ring potential 958 mV vs. SHE; ring and disk areas are 0.2471 cm^2 and 0.1867 cm^2, respectively; collection efficiency 37%.

To gain insight into the kinetics of the ORR on PNCEs, rotating ring disk electrode (RRDE) technique was applied to investigate the selectivity of the ORR on PNCEs-1000. In acid electrolyte, the ORR can proceed either by the direct 4-electron pathway to H_2O or via the 2-electron pathway to H_2O_2 (n=2). The preferred process for a good ORR catalyst is to reduce oxygen molecules directly to water via the 4-electron pathway. [42,43] Fig. 7 shows the ORR curves and H_2O_2 production rate of the PNCEs catalyst obtained at various rotation rates. The H_2O_2 yields gradually increases in the kinetic region (from 0.60 to 0.75 V, vs. SHE). The H_2O_2 generated rate changes from 1.11% -1.87%. The calculated n value is about 3.95-3.93 at potentials ranging from 0.60 V to 0.75 V, which proves the four-electron pathway.

Conclusions

In this work, nitrogen-doped carbon from PANI-PVP was synthesized by the polymerization process and the subsequently heat-treatment process under the NH_3 atmospheres. The catalysts were thoroughly characterized by X-ray diffraction, transmission electron microscopy, nitrogen adsorption, Raman spectroscopy and X-ray photoelectron spectroscopy (XPS). The role of the Fe species was investigated in detail by the XPS and XANES. Moreover, the ORR activities of the as-prepared catalyst were investigated by electrochemical measurements and single cells tests. The poison tolerance of methanol and SO_2 were also evaluated. The addition of PVP into the PANI can also significantly increase the surface area and tailor the pore structure as well as chemical components, which consequently improve the catalytic activity of the PNCEs. The heat-treatment temperatures chosen in this study are 700 °C, 800 °C, 900 °C, 1000 °C, and 1100 °C. The results demonstrate that the pyrolysis temperature and gas atmosphere play a crucial role in nitrogen species, nitrogen contents, and pore structures as well as the catalytic activity towards ORR of the PNCEs. The increase of the temperature yields the decrease of nitrogen content, in addition to the increase first and then decrease in pore volume and micropore surface area. The 1000°C is found to be the optimal carbonization temperature for obtaining the material with excellent catalytic activity. The maximum power density of the single cell with the PNCE prepared at 1000 °C as the cathode catalyst, W_{max}, is 456 mW cm^{-2} at the operating cell temperature of 80 °C. Moreover, PNCEs synthesized under NH_3 atmosphere displays higher activity than PNCEs prepared under nitrogen. Notably, the PNCE catalysts reveal superior stability to the commercial JM-20%Pt/C in 0.5 M H_2SO_4. It also exhibits excellent methanol and SO_2 tolerances. Furthermore, the results reveal that it is not the nitrogen content, but the nitrogen bonding configurations, textural structure, and surface areas of PNCEs as well as the Fe species play key roles in the electrocatalytic activity towards the ORR. This study provides us new choice of less expensive, efficient non-platinum catalysts in PEMFC, enhancing the commercialization prospects of the fuel cell technology.

Acknowledgements

The authors acknowledge financial support from the National Program on Key Basic Research Project (973 Program, 2012CB215500) and the National Natural Science Foundation of China (21006103). We would also greatly acknowledge the assistance from Beijing Synchrotron Radiation Facilities during the XANES tests. We thank Lirong Zheng, Min Wu and Zheng Tang for help in XANES tests. Thank Dr. Chuan Yao for drawing the scheme for the articles.

Notes and references

[a] *Division of Energy Storage, Dalian National Laboratory for Clean Energy (DNL), Dalian Institute of Chemical Physics, Chinese Academy of Sciences, Dalian 116023, China. Fax: 86-411-84665057; Tel: 86 -411-84379935; E-mail:zhonghexiang@dicp.ac.cn; zhanghm@dicp.ac.cn*

[b] *University of the Chinese Academy of Sciences, Beijing 100049, China.*

† Electronic Supplementary Information (ESI) available: [Complementary XPS spectra, BET, and XAFS for the catalyst]. See DOI: 10.1039/b000000x/

1 Handbook of Fuel Cells—Fundamentals Technology and Applications; vol. **3–4**, Part 3.

2 R. Borup, J. Meyers, B. Pivovar, Y. S. Kim, R. Mukundan, N.Garland, D. Myers, M.Wilson, F. Garzon, D. Wood, P. Zelenay, K. More, K.Stroh, T. Zawodzinski, J. Boncella, J. E. McGrath, M. Inaba, K. Miyatake, M. Hori, K. Ota, Z. Ogumi, S. Miyata, A. Nishikata, Z.Siroma, Y. Uchimoto, K.Yasuda, K. I. Kimijima and N. Iwashita, *Chem. Rev.* 2007, **107**, 3904.

3 (a) C. W. B. Bezerra, L. Zhang, H. S. Liu, K. C. Lee, A. L. B. Marques, E. P. Marques, H. J. Wang and J. J. Zhang, *Journal of*

Power Sources, 2007, **173**, 891; (b) Y. H. Bing, H.S.Liu, L. Zhang, D. Ghosh, J. Zhang, *Chem. Soc. Rev.* 2010, **39**, 2184.

4 (a) J. D.Wiggins-Camacho and K. J. Stevenson, *J. Phys. Chem. C*, 2009,**113**,19082; (b) M. K. Debe, *Nature*, 2012, **486**, 43.

5 (a) F. Xie, Z.G. Shao, J. X. Zhang, W.T. Lua, X.P. Qin, F.Lin, and B.L.Yi, *Electrochim. Acta,* 2012, **67**, 50; (b) Y. Garsany, O. A. Baturina and K.E.Swider-Lyons, *J. Electrochem. Soc.* 2009, **156**, B848.

6 (a) C. P. Ewels, M. Glerup, V. Krstic, V. A. Basiu, and E. V. Basiuk, *American Scientific Publishers* 2008, **3,** 65. (b) S.Angelika Wohlgemuth, F. Vilela, M.M. Titiricia and M. Antoniettia, *Green Chem.* 2012,**14**, 741.

7 K. K. R. Datta, V. V. Balasubramanian, K. Ariga, T. Mori and A. Vinu, *Chem. Eur.,* 2011, **17**, 3390.

8 L. F. Chen, X.D. Zhang, H.W. Liang, M. Kong, Q.F. Guan, P. Chen, Z.Y. Wu and S.H. Yu, *Acs Nano*, 2012, **6**, 7092.

9 K. P. Gong, F. Du, Z. H. Xia, M. Durstock and L. M. Dai, Science, 2009, **323**, 760.

10 (a) L. T. Qu, Y. Liu, J. B. Baek and L. M. Dai, Acs Nano, **4**, 1321. (b) Z. J. Wang, R. R. Jia, J. F. Zheng, J. G. Zhao, L. Li, J. L. Song and Z. P. Zhu, *Acs Nano*, 2011, **5**, 1677.

11 (a) N. Alonso-Vante, I. V. Malakhov, S. G. Nikitenko, E. R. Savinova and D. I. Kochubey, *Electrochim. Acta,* 2002**, 47**, 3807; (b) Y. Zhai, K. Bethune, G. Bender and R. Rocheleau, *J. Electrochem. Soc.*, 2012, **159,** B524.

12 N. P. Novák, K. Müller, K. S. V. Santhanam and O. Haas, *Chem. Rev.*, 1997, **97**, 207.

13 K. S. Kim and S. J. Park, *Microporous Mesoporous Mater.*, 2012, **163**, 140.

14 R. Silva, D. Voiry, M. Chhowalla and T. Asefa, *J. Am. Chem. Soc*, 2013, **135**, 7823.

15 H. Zhong, H. Zhang, Z. Xu, Y. Tang and J. Mao, *ChemSusChem*, 2012, **5**, 1698.

16 M. Lefevre, E. Proietti, F. Jaouen and J. P. Dodelet, *Science*, 2009, **324**, 71.

17 U. I. Kramm, M. Lefevre, N. Larouche, D. Schmeisser and J.P. Dodelet, *J.Am. Chem. Soc.*2014, **136**, 978

18 S. Maldonado, S. Morin and K. J. Stevenson, *Carbon*2006, *44*, 1429.

19 P. H. Matter, E. Wang, M. Arias, E. J. Biddinger and U. S. Ozkan, *J. Phys. Chem. B*2006, **110**, 18374-18384.

20 H. X. Zhong, H. M. Zhang, S. S. Liu, C. W. Deng and M. R. Wang, *Chemsuschem*, 2013, **6**, 807.

21 G. Wu, C. M. Johnston, N. H. Mack, K. Artyushkova, M. Ferrandon, M. Nelson, J. S. Lezama-Pacheco, S. D. Conradson, K. L. More, D. J. Myers and P. Zelenay, *J. Mater. Chem.*, 2011, **21**, 11392.

22 (a) G. Wu, K. L. More, C. M. Johnston and P. Zelenay, Science, 332, 443; (b) H. Peng, Z. Mo, S. Liao, H. Liang, L. Yang, F. Luo, H. Song, Y. Zhong and B. Zhang, *Scientific reports*, 2013, **3**, 1765.

23 (a) J. Fu, Q. Xu, J. Chen, Z. Chen, X. Huang and X. Tang, *Chem. Comm.*, 2010, **46**, 6563. (b) M. Kruk, M. Jaroniec and K.P.Gadkaree, *J. Colloid Interface Sci.*, 1997, **192**, 250.

24 G. P. Hao, W.C. Li, D. Qian and A.H. Lu, *Adv. Mater.*, 2010, **22**, 853.

25 S. J. Kim, K. S. Nahm and P. Kim, *Catal. Lett.,* 2012, **142**, 1244.

26 P. Yadav, A. Banerjee, S. Unni, J. Jog, S. Kurungot and S. Ogale, *ChemSusChem*, 2012, **5**, 2159.

27 J.Wu, Z. R.Yang, X. W. Li, Q. J. Sun, C. Jin, P. Strasser, R. Z.Yang, *J.Mater. Chem. A,* 2013, **1 (34)**, 9889.

28 C. H. Choi, M. W. Chung, S. H. Park and S. I. Woo, *RSC Adv.*, 2013, **3**, 4246.

29 S. Kundu, T. C. Nagaiah, W. Xia, Y. Wang, S. Van Dommele, J. H. Bitter, M. Santa, G. Grundmeier, M. Bron, W. Schuhmann and M. Muhler, *J. Phys. Chem. C*, 2009, **113**, 14302.

30 T. Sharifi, G. Hu, X. Jia and T. Wagberg, *Acs Nano*, 2012, **6**, 8904.

31 Y. Nabae, S. Moriya, K. Matsubayashi, S. M. Lyth, M. Malon, L. B. Wu, N. M. Islam, Y. Koshigoe, S. Kuroki, M. A. Kakimoto, S. Miyata and J. Ozaki, *Carbon*, 2010, **48**, 2613.

32 K. Kamiya, K. Hashimoto and S. Nakanishi, *Chem. Comm.*, 2012, **48**, 10213.

33 (a) J. L.Shui, N. K. K. Mahalingam, S.Y.Li, D.J. Liu, *J. Am. Chem. Soc.* 2012, **134**, 16654; (b) M. Ferrandon, A. J. Kropf, D. J. Myers, K. Artyushkova, U. Kramm, P. Bogdanoff, G. Wu, C. M. Johnston and P. Zelenay, *J. Phys. Chem. C*, 2012, **116**, 16001.

34 L. Lai, J. R. Potts, D. Zhan, L. Wang, C. K. Poh, C. Tang, H. Gong, Z. Shen, J. Lin and R. S. Ruoff, *Energy Environ. Sci.*, 2012, **5**, 7936.

35 D. W. Wang, F. Li, M. Liu, G. Q. Lu and H. M. Cheng, *Angew. Chem., Int. Ed.*, 2008, **47**, 373.

36 F. Su, C. K. Poh, J. S. Chen, G. Xu, D. Wang, Q. Li, J. Lin and X. W. Lou, *Energy Environ. Sci*, 2011, **4**, 717.

37 P. H. Matter, L. Zhang, U. S. Ozkan, *J. Catal.* 2006, **239 (1)**, 83; (b) P. H. Matter, E.Wang, M. Arias, E. J. Biddinger and U. S. Ozkan, *J. Mol. Catal. A-Chem.* 2007, **264**, 73; (c) E. J. Biddinger and U. S. Ozkan, *J. Phys. Chem. C*, 2010, **114**, 15306.

38 Z. Luo, S. Lim, Z. Tian, J. Shang, L.Lai, B. MacDonald, C. Fu, Z. Shen, T. Yu and J. Lin, *J. Mater. Chem.* 2011, **21**, 8038.

39 T. Ikeda, M. Boero, S. F. Huang, K. Terakura, M. Oshima and J. Ozaki, *J. Phys. Chem. C*, 2008, **112**, 14706.

40 L. Wang, J. Yin, L. Zhao, C. Tian, P. Yu, J. Wang and H. Fu, *Chem. Comm.,* 2013, **49**, 3022.

41 X. Wang and Y.S.Yan, *J. Electrochem Soc,* 2004, **151**, A2183.

42 L. Zhang, J. J. Zhang, D. P. Wilkinson and H. J. Wang, *J. Power Sources*, 2006, **156**, 171.

43 P. Wang, Z. K.Wang, L. X. Jia, Z. L. Xiao, *Phys. Chem. Chem. Phys.* 2009, **11**, 2730.